$4f^n \rightarrow 4f^{n-1}5d$ transitions of the heavy lanthanides: Experiment and theory

L. van Pieterson,[1] M. F. Reid,[2] G. W. Burdick,[3] and A. Meijerink[1]
[1]*Physics and Chemistry of Condensed Matter, Debye Institute, Utrecht University, P.O. Box 80 000, 3508 TA Utrecht, The Netherlands*
[2]*Department of Physics and Astronomy, University of Canterbury, Christchurch, New Zealand*
[3]*Department of Physics, Andrews University, Berrien Springs, Michigan 49104*
(Received 4 June 2001; revised manuscript received 28 August 2001; published 10 January 2002)

The $4f^n \rightarrow 4f^{n-1}5d(fd)$ excitation spectra of the heavy lanthanides (Tb^{3+}, Dy^{3+}, Ho^{3+}, Er^{3+}, Tm^{3+}, and Yb^{3+}) incorporated in $LiYF_4$, CaF_2, and YPO_4 are investigated in the ultraviolet and vacuum-ultraviolet spectral region (100–275 nm). Spin-forbidden transitions as well as spin-allowed transitions are observed for all heavy lanthanides. In the excitation spectra the crystal-field splitting of the $5d$ electron can be clearly observed. Fine structure (zero-phonon lines and vibronic lines) is observed for the transition to the lowest $5d$ crystal-field component, for both the high-spin and low-spin *fd* bands. Energy-level and intensity calculations are performed by an extension of the commonly used model for energy-level calculations of $4f^n$ states. A good agreement between experimental and simulated spectra is obtained, using parameters that describe the $5d$ crystal-field splitting (from the spectra of Ce^{3+}), the parameters for the splitting of the $4f^{n-1}$ core (from the literature on energy-level calculations for $4f^n$ states) and parameters for the spin-orbit coupling of the $5d$ electron and the Coulomb interaction between $4f$ and $5d$ electrons (from atomic *ab initio* calculations using the computer code of Cowan). To improve the agreement between the model and experiment, the $5d$ crystal-field parameters were adjusted slightly to correct for the decreasing crystal-field strength for the heavier rare earths due to the lanthanide contraction. The *f-d* interaction parameters in the fluoride host lattices were reduced to about 67% of the calculated free-ion values in order to compensate for the nephelauxetic effect.

DOI: 10.1103/PhysRevB.65.045114 PACS number(s): 78.40.Ha, 78.20.Bh, 71.55.−i, 71.70.Ch

I. INTRODUCTION

Recently, much progress in the calculation of the *fd* energy levels has been made. Calculations on the *fd* levels of Pr^{3+} (Ref. 1) and Ce^{3+}, Pr^{3+}, and Nd^{3+} (Ref. 2) in $LiYF_4$ have been reported. In the preceding paper we reported an extensive overview of the *fd* excitation spectra of the light lanthanides ($n<7$) incorporated in YPO_4, CaF_2, and $LiYF_4$ (Ref. 3). It was shown that the structure in the *fd* excitation spectra could be explained by extension of established models for the $4f^n$ configuration by including crystal-field and spin-orbit interactions for the $5d$ electron and the Coulomb interaction between the $4f$ and $5d$ electrons.

In this paper, study of the $4f^{n-1}5d$ energy levels is extended to the heavy lanthanide ions (Tb^{3+}, Dy^{3+}, Ho^{3+}, Er^{3+}, Tm^{3+}, and Yb^{3+}). The *fd* excitation spectra of the rare-earth (RE) ions incorporated in YPO_4, CaF_2, and $LiYF_4$ are reported. The choice of these host lattices is determined by the wide band gap, which makes it possible to observe *fd* excitation bands up to high energies. In addition, due to the weak ion-lattice coupling, fine structure (zero-phonon lines and vibronic lines) in the *fd* spectra can be observed. By recording excitation spectra using synchrotron radiation, high-resolution excitation spectra are obtained over the full range of interest (100–275 nm). Identification of the zero-phonon lines will give exact information on the energies of the electronic transitions and makes a comparison with energy-level calculations possible. It will be demonstrated that the energy levels and transition intensities of the $4f^n \rightarrow 4f^{n-1}5d$ transitions for the heavy lanthanides can be satisfactorily explained by extension of the standard model for energy-level calculations of $4f^n$ states.

An important difference in the spectra of the heavy ($n>7$) lanthanides as compared to the light ($n<7$) lanthanides is the observation of low-intensity bands on the low-energy side of the excitation spectra. The presence of spin-forbidden *fd* transitions have been known for a long time for Tb^{3+} (Ref. 4). Recently, these spin-forbidden *fd* bands have also been identified for all other heavy lanthanide ions. For the light lanthanides ($n<7$) spin-forbidden transitions are expected at higher energy than the spin-allowed transitions and cannot be clearly observed in the excitation spectra. The occurrence of both spin-forbidden and spin-allowed *fd* transitions complicates the *fd* structure in the excitation spectra of the heavy lanthanides and detailed calculations are needed to account for all observed bands. On the other hand, the splitting between the low-spin (LS) and high-spin (HS) *fd* state provides extra information. The LS-HS splitting is mainly caused by the Coulomb interaction between the $4f$ electrons and the $5d$ electron. The LS-HS splitting for the heavy lanthanides in a host lattice is reduced in comparison with the free-ion situation. Due to the nephelauxetic effect the interaction between the (delocalized) $5d$ electron and the $4f^{n-1}$ core is reduced. Experimental observations on the LS-HS splitting make it possible to estimate the reduction of the free-ion *f-d* interaction parameters from the theoretical values calculated with Cowan's atomic physics computer program.[5]

II. MODEL

An extensive description of the model has been given in an earlier paper[2] and the preceding paper. To calculate the $4f^{n-1}5d$ energy levels the established theoretical models for $4f^n$ energy levels are extended to include the splitting of the $5d$ state (by the crystal-field and the spin-orbit coupling) and

the interaction between the $4f^{n-1}$ and $5d$ configuration.

In our calculations we used $4f^n$ crystal-field parameters[6–8] and $4f^n$ atomic parameters[9] from the literature. If no data in the literature were available on the $4f^n$ crystal-field parameters for a certain rare-earth ion in a host lattice, the crystal-field parameters of a neighbor ion in the same host lattice were used. *Ab initio* $4f^n$ atomic parameters were calculated for both the free-ion $4f^n$ and $4f^{n-1}5d$ configuration. In comparison with our previous papers[2,3] some improvements of the model are included here. The $4f^n$ atomic parameters are predicted to be slightly larger in the $4f^{n-1}5d$ configuration than in the $4f^n$ configuration ($\sim$1.06 times). This can be understood in terms of increased Coulomb interaction for the contracted $4f^{n-1}$ core. To take this effect into account, we multiplied the literature $4f^n$ atomic parameters by a small factor (1.06) for the excited $4f^{n-1}5d$ configuration. For the *f-d* interaction parameters we used atomic (Coulomb and spin-orbit) parameters calculated from standard atomic computer programs.[5] The atomic Coulomb *fd* parameters were reduced to approximately 67% of the calculated value to correct for delocalization of the $5d$ electron over the ligands (nephelauxetic effect), which will reduce the *f-d* coupling parameters in comparison to the free-ion situation.[10] As was indicated in the introduction, the experimentally observed HS-LS splitting makes it possible to make a good estimate of the reduction. The $5d$ crystal-field parameters were obtained from fits to the Ce^{3+} spectrum[3] and were reduced slightly (5–9%, from Tb^{3+} to Tm^{3+}) to correct for the decreasing crystal-field strength observed for the heavier lanthanide ions due to the lanthanide contraction.

III. RESULTS

In this section the experimentally recorded excitation spectra of the various heavy lanthanides in YPO_4, CaF_2, and $LiYF_4$ are reported and discussed. The experimental techniques used to prepare the samples and the equipment used to record the spectra are the same as those described in the preceding article.[3] To explain the experimentally observed spectra energy-level calculations have been performed for most ions in $LiYF_4$, CaF_2, and YPO_4. A comparison between the measured and calculated spectra is made and discussed for each ion separately. In the subsequent section a general discussion of energy-level calculations for the heavy lanthanides in the three host lattices is presented.

A. Tb^{3+}

The ground configuration of the Tb^{3+} ion is $4f^8$. The excited configuration is $4f^75d^1$, in which the $4f$ shell is half-filled. Because the lowest excited $4f$ level within the $4f^7$ configuration is located at very high energy (32 000 cm^{-1} for Gd^{3+}), the *fd* excitation spectrum of Tb^{3+} is expected to be quite similar to that of Ce^{3+} ($4f^05d^1$ configuration in the excited state) showing excitation bands corresponding to the different $5d$ states. However, the interaction between the seven $4f$ electrons and the $5d$ electron will give rise to a more complicated spectrum. As discussed in Sec. I, spin-forbidden *fd* transitions can be expected in addition to spin-allowed transitions.

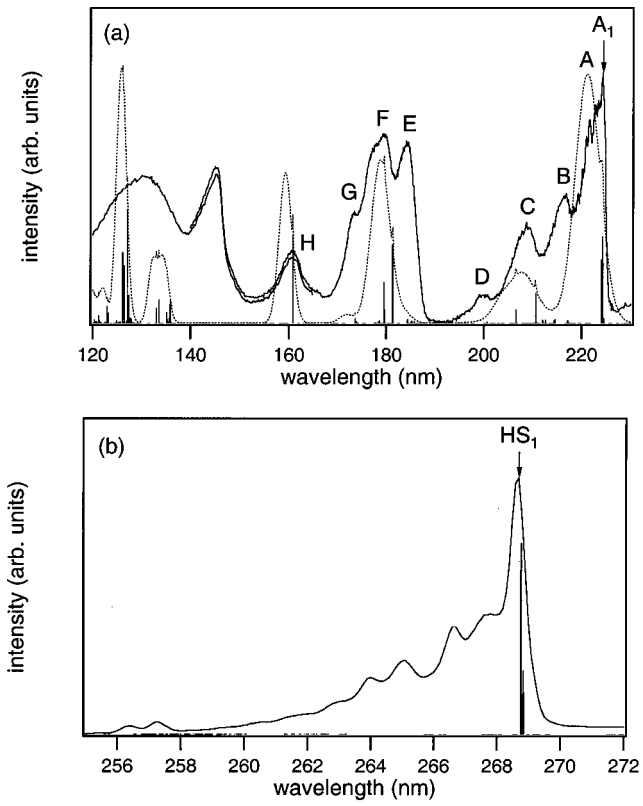

FIG. 1. (a) Excitation spectrum for YPO_4 doped with 1% Tb^{3+} recorded monitoring the $^5D_4 \rightarrow {}^7F_5$ emission at 544 nm at 6 K. The solid line shows the excitation spectrum measured at the DESY synchrotron, the dotted line represents the calculated spectrum. Positions of the calculated electronic states are indicated by sticks to the horizontal axis. The height of the sticks is proportional to the calculated intensity. (b) Excitation spectrum for YPO_4 doped with 1% Tb^{3+} recorded monitoring the $^5D_4 \rightarrow {}^7F_5$ emission at 544 nm at 6 K at the SPEX, showing the energy region in which the transition to the high-spin *fd* state is observed.

1. Experiment

YPO_4. Figure 1(a) shows the excitation spectrum of YPO_4 doped with 1% Tb^{3+}. A number of broad bands are observed with maxima at 223 nm (A), 217 nm (B), 209 nm (C), 200 nm (D), 184 nm (E), 179 nm (F), 173 nm (G), and 161 nm (H). The lower-energy part of the spectrum is in good agreement with the high resolution spectra reported for YPO_4:Tb^{3+} by Hoshina.[11] At about 144 nm the YPO_4 host lattice excitation edge is observed, which indicates that energy transfer from the host lattice to Tb^{3+} is possible or that host lattice defect emission is monitored simultaneously at this wavelength (540 nm). It is known that YPO_4 shows a broad defect emission band with a maximum at 440 nm.[12] Excitation over the band gap of the YPO_4 host ($\lambda = 144$ nm) gives Tb^{3+} $4f^n \rightarrow 4f^n$ line emission on top of a broad defect emission, which shows that energy transfer from YPO_4 to Tb^{3+} is inefficient. Because the tail of the defect emission is monitored at 540 nm and because Tb^{3+} emission is observed around 540 nm upon excitation over the band gap, the band edge is observed in the excitation spectrum in Fig. 1(a). Comparison with the excitation spectrum

of YPO_4:Ce^{3+} (Ref. 3) shows that bands A, E, F, G, and H correspond to the spin-allowed transitions to the five $5d$ crystal-field components. The crystal-field splitting for Tb^{3+} in YPO_4 is somewhat smaller than for Ce^{3+} (about 3–5% smaller). This is explained by the slightly smaller ionic radius of the Tb^{3+} ion (1.18 Å in VIII coordination vs 1.28 Å for Ce^{3+} in VIII coordination), which reduces the crystal-field strength. Additional bands between 190 and 218 nm (B–D) are observed in the excitation spectrum of Tb^{3+} and not in the Ce^{3+} spectrum. These bands are due to interaction of the $4f$ electrons with the $5d$ electron.

Just as was observed for the light lanthanides,[3] the lowest-energy *fd* excitation band (A) of Tb^{3+} shows fine structure. It consists of a zero-phonon line at 224.3 nm (A_1) and a vibronic side band. For the transitions to the higher energy $5d$ levels no fine structure was observed. The electronic origins of these transitions are thought to be broadened due to photoionization to the conduction band.

For RE ions with more than seven $4f$ electrons, spin-forbidden (high spin) *fd* bands can be observed in addition to the already mentioned spin-allowed (low spin) *fd* transitions. Figure 1(b) shows the lowest energy HS *fd* excitation band of YPO_4:Tb^{3+}. The spectrum agrees with the high-resolution spectrum reported by Hoshina for the spin-forbidden *fd* transition for Tb^{3+} in YPO_4.[11] Just as for the lowest-energy spin-allowed transition, fine structure is observed. It consists of a zero-phonon line at 268.7 nm (HS_1) and a vibronic side band. The progression is similar to vibronic patterns observed for the LS *fd* bands of the light lanthanides.[3] The energy separation between the LS *fd* transition and the HS *fd* transition of Tb^{3+} ($A_1 - HS_1$) is 7370 cm^{-1}.

Transitions to the higher-energy HS $5d$ crystal-field components are expected to have a much lower intensity than the LS *fd* bands, because they are spin forbidden. The bands between 190 and 218 nm (bands B, C, and D) can be explained by transitions to states arising from interactions between the $4f^7$ core and the $5d$ electron (see below).

CaF_2. Figure 2(a) shows the excitation spectrum of the Tb^{3+} emission for CaF_2 doped with 0.1% Tb^{3+}. To minimize the influence of saturation due to the relative high dopant concentration, the single crystal was powdered. Unlike other CaF_2 crystals discussed in this work, this crystal was not grown in the presence of Na^+ charge compensation ions and therefore a different distribution of sites can be expected than for the other RE ions in CaF_2 discussed in this paper. For CaF_2 crystals slowly cooled to room temperature in the absence of a charge compensator, C_{4v} and C_{3v} sites are known to dominate.[13] For the smaller heavy lanthanides C_{3v} sites are predicted to be more stable.[14] FTIR spectra of our crystal show that the trigonal site is indeed dominant.

The excitation spectrum of the Tb^{3+} emission at 388 nm shows only a few bands with maxima at 215 nm (A), 154 nm (B), 132 nm (C), and 125 nm (D). This spectrum differs from the absorption spectrum reported in Ref. 15, where many bands between 160 and 200 nm were observed. The Tb^{3+} concentration used in Ref. 15 is similar to ours (0.1%), but the absorption spectrum of a crystal was measured. At concentrations higher than 0.05%, cluster sites exist in CaF_2 in addition to single-ion sites. In an absorption spectrum, all sites will be observed, while in an excitation spectrum a single type of site can be selectively measured by choosing a proper emission wavelength. The presently chosen emission wavelength (388 nm) corresponds to a transition from the $^5D_3$ level ($^5D_3 \rightarrow {}^7F_6$). In cluster sites this emission will be efficiently quenched by cross relaxation and only $^5D_4$ emission is observed for Tb^{3+} cluster sites. As a result only the excitation spectrum of single ion sites is obtained by measuring the excitation spectrum for emission at 388 nm.

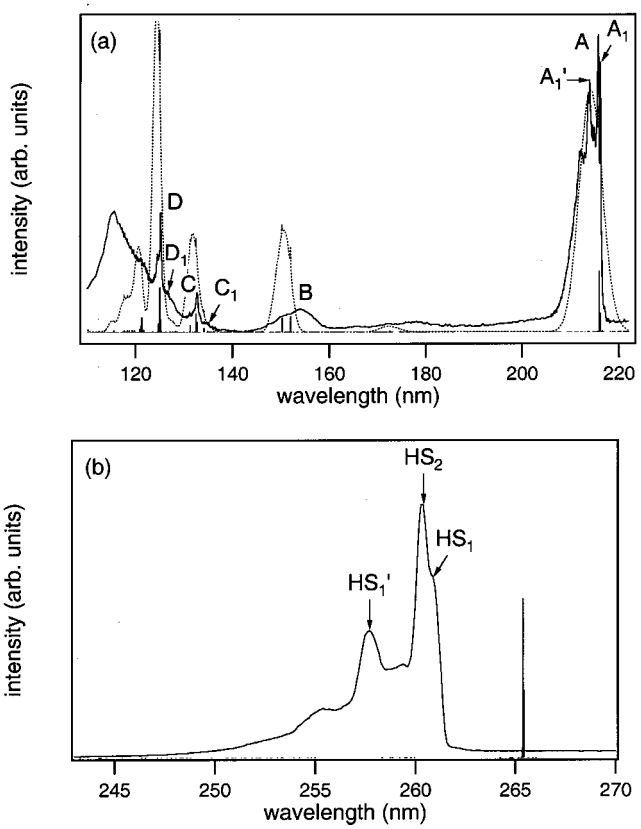

FIG. 2. Excitation spectrum for powdered CaF_2 doped with 0.1% Tb^{3+} recorded monitoring the $^5D_3 \rightarrow {}^7F_6$ emission at 388 nm at 10 K. The solid line in (a) shows the excitation spectrum measured at DESY, the dotted line represents the calculated spectrum. (b) Excitation spectrum for a CaF_2 crystal doped with 0.1% Tb^{3+} recorded monitoring the $^5D_4 \rightarrow {}^7F_5$ emission at 544 nm at 6 K at the SPEX, showing the energy region in which the transition to the high-spin *fd* state is observed.

The $5d$ states are split by the crystal-field and spin-orbit coupling. The band at 215 nm (A) shows fine structure and is assigned to the transition to the lower-energy ^2E levels. The broad band at 154 nm (B) is assigned to transitions to the higher-energy $^2T_2$ levels. Splitting of the ^2E and $^2T_2$ bands due to lowering of the site symmetry from cubic to C_{3v} and spin-orbit coupling results in a broadening of the band, rather than the observation of separate bands.

The transition to the lowest energy (LS) *fd* band (band A) shows fine structure and consists of a zero-phonon line at 216.23 nm (A_1) and a vibronic side band. The energy separation between A_1 and A_1' is about 470 cm^{-1} and may be explained in terms of phonon frequencies corresponding to

local modes involving the Tb^{3+} ion, such as the local breathing mode oscillations of the eight fluoride ions surrounding the RE ion.[21] The position of the zero-phonon line A_1 (at 216.23 nm) does not agree with the position of the Tb^{3+} fd zero-phonon line reported in the literature (217.07 nm).[15] However, FTIR measurements showed that in our crystal C_{3v} is the dominant site, whereas in Ref. 15 absorption of C_{4v} sites was reported.

The band corresponding to the transitions to the ^2E levels at 154 nm (B) does not show fine structure, which is explained by assuming that these levels are located in the conduction band. Fast photoionization to resonant levels in the conduction band causes Heisenberg broadening of the electronic origins of these transitions and explains the absence of fine structure. However, at 132 and 125 nm (bands C and D) again two structured bands are observed. The energy separation between C_1 and A_1 is about 28 000 cm^{-1} and between D_1 and A_1 is about 33 000 cm^{-1}. The reappearance of fine structure suggests that the bands around 132 and 125 nm correspond to transitions to states involving the lowest-energy $5d$ state and high-energy excited states in the $4f^7$ core. The splittings between C_1-A_1 and D_1-A_1 match the splittings ^8S-^6P and ^8S-^6I for the $4f^7$ core quite closely. The reappearance of fine structure is observed in other systems as well and will be discussed in more detail in Ref. 16.

In the excitation spectrum of powdered CaF_2 doped with 0.1% Tb^{3+}, no bands due to spin-forbidden transitions are observed. Apparently, the intensity of these high-spin *fd* bands is too low to be observed for the powdered sample. Figure 2(b) shows the excitation spectrum of a CaF_2:Tb^{3+} 0.1% crystal. In this spectrum the lowest-energy spin-forbidden *fd* transition is observed as a structured band around 260 nm. It consists of a zero-phonon line and a vibronic side band. The resolution of the spectrum is not very high, zero-phonon line HS_1 (at 260.9 nm) is observed as a shoulder on the more intense line HS_2. The vibronic replica HS_1' is at about 475 cm^{-1} higher energy and is assigned to the breathing mode oscillations of the fluoride ions surrounding Tb^{3+} (Ref. 15). The energy separation between the lowest energy LS and HS *fd* excitation band of Tb^{3+} in CaF_2 is calculated from the positions of the zero-phonon lines in Figs. 2(a) and 2(b) and is about 7920 cm^{-1}. This is similar, although slightly larger, to the energy separation between the LS and HS *fd* bands in YPO_4.

$LiYF_4$. Figure 3 shows the excitation spectrum of the Tb^{3+} $^5D_4 \rightarrow {}^7F_5$ emission at 545 nm in powdered $LiYF_4$ doped with 1% Tb^{3+}. A large number of bands are observed. The lowest-energy spin-allowed *fd* excitation band is located at 212 nm (A). From analysis of the spectrum of Ce^{3+} incorporated in $LiYF_4$, it is known that due to the S_4 site symmetry and the spin-orbit coupling the $5d$ state is split into five levels. Comparison of the spectrum of $LiYF_4$:Tb^{3+} with that of Ce^{3+} in $LiYF_4$,[3] shows that the bands with maxima at 211 nm (A), 182 nm (C), 160 nm (F), 154 nm (G), and 151 nm (H) can be assigned to the spin-allowed transitions to the five $5d$ crystal-field components. The crystal-field splitting is slightly reduced compared to the splitting observed for Ce^{3+}, due to the smaller ionic radius of Tb^{3+}. Other bands in the

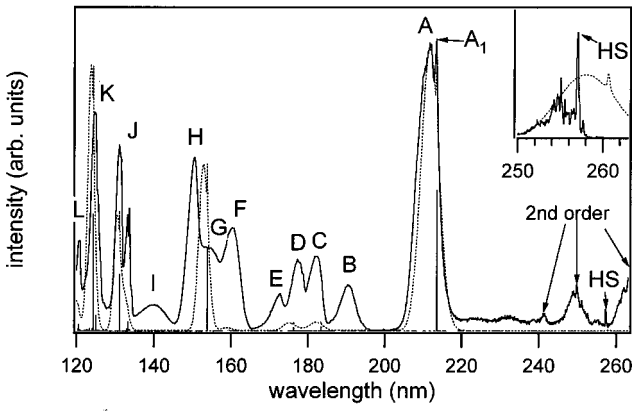

FIG. 3. Excitation spectrum for $LiYF_4$ doped with 1% Tb^{3+} recorded monitoring the $^5D_4 \rightarrow {}^7F_5$ emission at 544 nm at 10 K. In the inset a high-resolution excitation spectrum for $LiYF_4$:Tb^{3+} is shown recorded monitoring the $^5D_4 \rightarrow {}^7F_5$ emission at 544 nm at 10 K using a tunable laser setup.

spectrum, which are not observed in the spectrum of $LiYF_4$:Ce^{3+} (bands B, D, and E), arise from the interaction of the $4f$ electrons with the $5d$ electron.

The lowest energy LS *fd* band (A) shows fine structure and consists of a zero-phonon line at 213.4 nm (indicated A_1) and a vibronic side band. The vibronic structure is not well resolved. For transitions to the higher energy $5d$ states fine structure disappears, as is usually observed. Just as for Tb^{3+} in CaF_2, fine structure reappears in the high-energy bands around 130 nm. As indicated above, this surprising observation will be discussed in Ref. 16.

Most of the bands on the low-energy side of the spectrum are second order bands of the transitions measured at shorter wavelengths in the spectrum. An exception is the low intensity peak at 257 nm (HS). In the inset of Fig. 3 a high resolution excitation spectrum recorded with a tunable laser setup is given. The electronic origin of the lowest energy spin-forbidden transition to the HS $4f^7 5d$ state (HS_1) is observed at 257.25 nm. The energy difference between the low-spin and high-spin *fd* state is 7995 cm^{-1}, similar to the splitting observed in YPO_4 and CaF_2.

2. Model

The structure observed in the excitation spectra of the Tb^{3+} emission in YPO_4, CaF_2, and $LiYF_4$ is very similar. The splitting of the $5d$ state is observed, similar to the structure observed for Ce^{3+}. The crystal-field splitting is slightly reduced in comparison with Ce^{3+}. In addition, extra bands are observed arising from interaction between the $4f^7$ core and the $5d$ electron. This interaction gives rise to high spin and low spin $4f^7 5d$ states. The splitting between the lowest energy HS and LS state is just below 8000 cm^{-1} for Tb^{3+} in all three host lattices.

Energy level calculations as outlined in Sec. II were performed. In general, the energy level calculations require as input parameters the crystal-field and spin-orbit parameters for the $5d$ electron, the parameters for the splitting of the $4f^{n-1}$ core and parameters for Coulomb interaction of the f

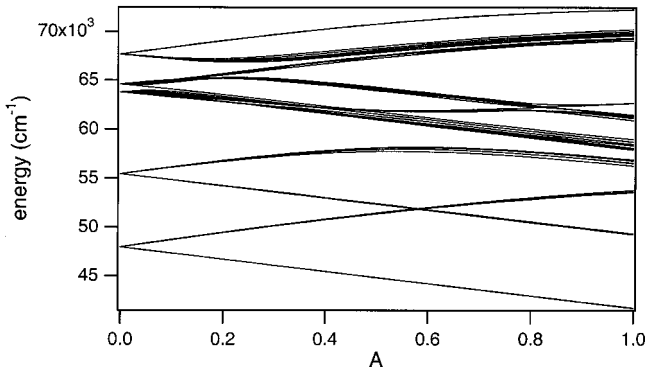

FIG. 4. Splitting of the five $4f^7 5d$ crystal-field states of Tb^{3+} in $LiYF_4$. The parameter *A* represents the *f-d* interactions as explained in the text. On the left ($A=0$) the parameters for these interactions are set to zero and on the right ($A=1$) they have the values calculated for the free ion.

and *d* electrons. The $5d$ crystal-field parameters are taken from the analysis of the Ce^{3+} spectrum[3] and are reduced slightly (approximately 5%) to account for the weaker crystal-field experienced by Tb^{3+} as compared to Ce^{3+} due to the lanthanide contraction. The observed crystal-field splitting for the lanthanides decreases gradually by about 9% through the series from Ce^{3+} to Tm^{3+}. In this paper, the reduction of the crystal field parameters is assumed to be continuous between Ce^{3+} and Tm^{3+} and the parameters are obtained by extrapolation assuming a 9% reduction for Tm^{3+}. For the splitting of the $4f^{n-1}$ core, parameters were taken from the literature of the $4f^n$ ion ($4f^8$ for Tb^{3+} spectra) and were multiplied a factor 1.06 (see Sec. II). The parameters for the *f-d* Coulomb interaction were estimated using Cowan's code,[5] but were reduced to 67% of the calculated free ion value in order to predict a correct splitting between the high spin and low spin state. The reduction factor was estimated in the following way.

Figure 4 shows the splitting of the five $5d$ crystal-field states as the *f-d* interaction parameters $[F^k(fd), G^j(fd)]$ are increased from zero to the values predicted for the free ion according to Cowan's program.[5] The parameter A used as the horizontal axis of the graph multiplies the *f-d* parameters calculated for the free ion value. When $A=0$, which corresponds to setting the *f-d* interaction parameters equal to zero, five $5d$ crystal-field levels are observed. As A is increased from 0 to 1 the Coulomb interaction between the $4f$ electrons and the $5d$ electron splits the $4f^7 5d$ states in high-spin and low-spin states. When we compare the splitting of 11 700 cm^{-1} for $A=1$ between the LS and HS states of the lowest $4f^7 5d$ level in Fig. 4 with the experimentally observed splitting of about 8000 cm^{-1} between the high-spin and low-spin *fd* state, it is clear that the *fd* parameters predicted for the free ion should be reduced in order to reproduce the experimentally observed energy difference between both states. A reduction of the *f-d* interaction parameters for ions in a lattice is expected: due to the nephelauxetic effect the $5d$ orbitals will be partly delocalized over the ligands, thus reducing the interaction with the $4f$ core. In our previous paper on the *fd* levels of the light lanthanides it was shown that a reduction of the *f-d* interaction parameters leads to a significantly better agreement between theory and experiment.[3] The observation of high-spin and low-spin *fd* bands makes it possible to obtain a good estimate for the reduction of the *f-d* interaction parameters for the heavy lanthanides. From Fig. 4 and similar figures for the other lanthanides, we found that a reduction of the calculated parameters to about 67% gives the best overall agreement between the observed and calculated HS-LS splittings. This is in line with the value of 74% which was found to give the best agreement between experiment and model for the (larger) Nd^{3+} ion in $LiYF_4$ (Ref. 3).

In view of the similar covalency of $LiYF_4$ and CaF_2 (both fluoride host lattices) a similar reduction of the *f-d* interaction parameters (67%) was used for CaF_2. The YPO_4 host lattice is more covalent and therefore the delocalization of the $5d$ electron over the ligands will be larger than in the fluoride lattices. From the smaller splitting between the high-spin and low-spin states of Tb^{3+} in YPO_4 as compared to $LiYF_4$ (7370 cm^{-1} in YPO_4 vs 7995 cm^{-1} in $LiYF_4$), a reduction of the *f-d* interaction parameters to 60% of the calculated free ion values was estimated for the lanthanides in YPO_4.

The calculated spectra are shown as the dotted line in Figs. 1(a), 2(a), and 3. All parameters used in the calculations are summarized in Table I. For CaF_2:Tb^{3+} parameters determined for cubic symmetry are used for consistency with the parameters used for the other RE ions in this paper (see below). Since the deviation of the C_{3v} symmetry from cubic symmetry is relatively small no large errors are introduced. The agreement between experiment and model is good. Both spin-allowed and spin-forbidden transitions are predicted by the theory. In the spectra of Tb^{3+} in YPO_4 and $LiYF_4$ [Figs. 1(a) and 3], the splitting of the high-energy $5d$ crystal-field components [bands E and F in Fig. 1(a) and bands F, G, and H in Fig. 3], is not well reproduced. This was also observed for the light lanthanides[3] and is partly due to the fact that the $5d$ crystal-field splitting for these higher-energy crystal-field components cannot be reproduced by the fits for YPO_4:Ce^{3+} and $LiYF_4$:Ce^{3+}. This discrepancy was thought to be a result of distortions in the excited state.[17] All other excitation bands, including the bands showing fine structure around 130 nm in the spectra of CaF_2:Tb^{3+} and $LiYF_4$:Tb^{3+}, are well reproduced by the energy-level calculations, with the exception of band I in Fig. 3. The origin of this band is not clear. In view of the large width, this rather weak band may be related to a defect or impurity, and not to Tb^{3+}.

B. Dy^{3+}

1. Experiment

YPO_4. Figure 5 shows the excitation spectrum of YPO_4 doped with 1% Dy^{3+} ($4f^9$) monitoring the $^4F_{9/2} \rightarrow {}^6H_{15/2}$ emission at 478 nm. The spin-allowed *fd* onset is observed at 176.69 nm (A_1). The host lattice excitation edge is observed at 144 nm (C). Transitions to the higher-energy crystal-field components are expected between 140 and 151 nm, but are not observed in the spectrum. Probably the competing absorption by (defects in) the host lattice is too large.

TABLE I. Parameters used for energy-level calculations for $4f^n$ and $4f^{n-1}5d$ configurations of Tb^{3+}, Dy^{3+}, Ho^{3+}, Er^{3+}, and Tm^{3+} in YPO_4, CaF_2 and $LiYF_4$. Parameters for the splitting of the $4f^{n-1}$ core (such as Coulomb interaction, spin-orbit interaction, and crystal-field splitting) are obtained from the literature[6–9] ($4f^n$ atomic parameters for the excited $4f^{n-1}5d$ state are multiplied by ~1.06). The *f-d* interaction parameters are calculated for the free ion using Cowan's code (Ref. 5) and reduced to correct for the nephelauxetic effect. For the crystal-field splitting of the $5d$ state, parameters are obtained from the fits of the Ce^{3+} spectra[3] and are reduced slightly to correct for the decreasing crystal field strength in the lanthanide series. Further details are provided in the text. Units are in cm^{-1}.

	Tb^{3+}			Dy^{3+}			Ho^{3+}		Er^{3+}		Tm^{3+}	
	YPO_4	CaF_2	$LiYF_4$	YPO_4	CaF_2	$LiYF_4$	CaF_2	$LiYF_4$	CaF_2	$LiYF_4$	CaF_2	$LiYF_4$
$F^2(ff)$	94335 (Ref. 9)	94335 (Ref. 9)	94335 (Ref. 9)	97417 (Ref. 9)	97417 (Ref. 9)	94717 (Ref. 9)	100238 (Ref. 9)	100238 (Ref. 9)	103332 (Ref. 9)	103332 (Ref. 9)	108145 (Ref. 9)	108145 (Ref. 9)
$F^4(ff)$	66694 (Ref. 9)	66694 (Ref. 9)	66694 (Ref. 9)	68234 (Ref. 9)	38234 (Ref. 9)	68234 (Ref. 9)	70381 (Ref. 9)	70381 (Ref. 9)	71978 (Ref. 9)	71798 (Ref. 9)	75182 (Ref. 9)	75182 (Ref. 9)
$F^6(ff)$	50087 (Ref. 9)	50087 (Ref. 9)	50087 (Ref. 9)	52349 (Ref. 9)	52349 (Ref. 9)	52349 (Ref. 9)	55143 (Ref. 9)	55143 (Ref. 9)	57251 (Ref. 9)	57251 (Ref. 9)	60453 (Ref. 9)	60453 (Ref. 9)
$\alpha(ff)$	18.4 (Ref. 9)	18.4 (Ref. 9)	18.4 (Ref. 9)	18.02 (Ref. 9)	18.02 (Ref. 9)	18.02 (Ref. 9)	17.15 (Ref. 9)	17.15 (Ref. 9)	17.79 (Ref. 9)	17.79 (Ref. 9)	17.26 (Ref. 9)	17.26 (Ref. 9)
$\beta(ff)$	−590.9 (Ref. 9)	−590.9 (Ref. 9)	−590.9 (Ref. 9)	−633.4 (Ref. 9)	−633.4 (Ref. 9)	−633.4 (Ref. 9)	−607.9 (Ref. 9)	−607.9 (Ref. 9)	−582.1 (Ref. 9)	−582.1 (Ref. 9)	−624.5 (Ref. 9)	−624.5 (Ref. 9)
$\gamma(ff)$	1650 (Ref. 9)	1650 (Ref. 9)	1650 (Ref. 9)	1790 (Ref. 9)	1790 (Ref. 9)	1790 (Ref. 9)	1800 (Ref. 9)	1800 (Ref. 9)	1800 (Ref. 9)	1800 (Ref. 9)	1820 (Ref. 9)	1820 (Ref. 9)
$T_2(ff)$	320 (Ref. 9)	320 (Ref. 9)	320 (Ref. 9)	329 (Ref. 9)	329 (Ref. 9)	329 (Ref. 9)	400 (Ref. 9)	400 (Ref. 9)	400 (Ref. 9)	400 (Ref. 9)		
$T_3(ff)$	40 (Ref. 9)	40 (Ref. 9)	40 (Ref. 9)	36 (Ref. 9)	36 (Ref. 9)	36 (Ref. 9)	37 (Ref. 9)	37 (Ref. 9)	43 (Ref. 9)	43 (Ref. 9)		
$T_4(ff)$	50 (Ref. 9)	50 (Ref. 9)	50 (Ref. 9)	127 (Ref. 9)	127 (Ref. 9)	127 (Ref. 9)	107 (Ref. 9)	107 (Ref. 9)	73 (Ref. 9)	73 (Ref. 9)		
$T_6(ff)$	−395 (Ref. 9)	−395 (Ref. 9)	−395 (Ref. 9)	−314 (Ref. 9)	−314 (Ref. 9)	−314 (Ref. 9)	−264 (Ref. 9)	−264 (Ref. 9)	−271 (Ref. 9)	−271 (Ref. 9)		
$T_7(ff)$	303 (Ref. 9)	303 (Ref. 9)	303 (Ref. 9)	404 (Ref. 9)	404 (Ref. 9)	404 (Ref. 9)	316 (Ref. 9)	316 (Ref. 9)	308 (Ref. 9)	308 (Ref. 9)		
$T_8(ff)$	317 (Ref. 9)	317 (Ref. 9)	317 (Ref. 9)	315 (Ref. 9)	315 (Ref. 9)	315 (Ref. 9)	336 (Ref. 9)	336 (Ref. 9)	299 (Ref. 9)	299 (Ref. 9)		
$\varsigma(ff)$	1707 (Ref. 9)	1707 (Ref. 9)	1707 (Ref. 9)	1913 (Ref. 9)	1913 (Ref. 9)	1913 (Ref. 9)	2145 (Ref. 9)	2145 (Ref. 9)	2376 (Ref. 9)	2376 (Ref. 9)	2636 (Ref. 9)	2636 (Ref. 9)
$M_0(ff)$[a]	2.39 (Ref. 9)	2.39 (Ref. 9)	2.39 (Ref. 9)	3.39 (Ref. 9)	3.39 (Ref. 9)	3.39 (Ref. 9)	2.54 (Ref. 9)	2.54 (Ref. 9)	3.86 (Ref. 9)	3.86 (Ref. 9)	3.81 (Ref. 9)	3.81 (Ref. 9)
$P_2(ff)$[b]	373 (Ref. 9)	373 (Ref. 9)	373 (Ref. 9)	719 (Ref. 9)	719 (Ref. 9)	719 (Ref. 9)	605 (Ref. 9)	605 (Ref. 9)	594 (Ref. 9)	594 (Ref. 9)	695 (Ref. 9)	695 (Ref. 9)
$B_0^2(ff)$	352 (Ref. 8)		400 (Ref. 6)	352 (Ref. 8)		340 (Ref. 6)		408 (Ref. 5)		352 (Ref. 6)		348 (Ref. 6)
$B_0^4(ff)$	112 (Ref. 8)	−2185 (Ref. 7)	−802 (Ref. 6)	112 (Ref. 8)	−2185 (Ref. 7)	−784 (Ref. 6)	−1906 (Ref. 7)	−629 (Ref. 6)	−1906 (Ref. 7)	−820 (Ref. 6)	−1906 (Ref. 7)	−639 (Ref. 6)
$B_4^4(ff)$	−800 (Ref. 8)	−1305 (Ref. 7)	−1055 (Ref. 6)	−800 (Ref. 8)	−1305 (Ref. 7)	−951 (Ref. 6)	−1139 (Ref. 7)	−835 (Ref. 6)	−1139 (Ref. 7)	−1000 (Ref. 6)	−1139 (Ref. 7)	−864 (Ref. 6)
$B_0^6(ff)$	−848 (Ref. 8)	733.6 (Ref. 7)	−57 (Ref. 6)	−848 (Ref. 8)	−733.6 (Ref. 7)	−7 (Ref. 6)	−650.5 (Ref. 7)	−18 (Ref. 6)	650.5 (Ref. 7)	−134 (Ref. 6)	650.5 (Ref. 7)	−182 (Ref. 6)
$B_4^6(ff)$	151 (Ref. 8)	−1372 (Ref. 7)	−754 (Ref. 6)	151 (Ref. 8)	−1372 (Ref. 7)	−850 (Ref. 6)	−1216 (Ref. 7)	−673 (Ref. 6)	−1216 (Ref. 7)	−617 (Ref. 6)	−1216 (Ref. 7)	−641 (Ref. 6)
$\Delta_E(fd)$	79016	81991	81899	81796	86013	85738	91322	89516	92508	92216	94783	95091
$F^2(fd)$	17877 (Ref. 5)	19665 (Ref. 5)	19665 (Ref. 15)	17809 (Ref. 5)	19886 (Ref. 5)	19886 (Ref. 5)	19807 (Ref. 5)	19807 (Ref. 5)	19724 (Ref. 5)	19724 (Ref. 5)	19639 (Ref. 5)	19639 (Ref. 5)
$F^4(fd)$	8608 (Ref. 5)	9469 (Ref. 5)	9469 (Ref. 5)	8531 (Ref. 5)	9527 (Ref. 5)	9527 (Ref. 5)	9442 (Ref. 5)	9442 (Ref. 5)	9358 (Ref. 5)	9358 (Ref. 5)	9275 (Ref. 5)	9275 (Ref. 5)
$G^1(fd)$	7348 (Ref. 5)	8083 (Ref. 5)	8083 (Ref. 5)	7294 (Ref. 5)	8145 (Ref. 5)	8145 (Ref. 5)	8089 (Ref. 5)	8089 (Ref. 5)	8038 (Ref. 5)	8038 (Ref. 5)	7991 (Ref. 5)	7991 (Ref. 5)
$G^3(fd)$	6305 (Ref. 5)	6935 (Ref. 5)	6935 (Ref. 5)	6245 (Ref. 5)	6973 (Ref. 5)	6973 (Ref. 5)	6910 (Ref. 5)	6910 (Ref. 5)	6848 (Ref. 5)	6848 (Ref. 5)	6789 (Ref. 5)	6789 (Ref. 5)
$G^5(fd)$	4888 (Ref. 5)	5376 (Ref. 5)	5376 (Ref. 5)	4836 (Ref. 5)	5400 (Ref. 5)	5400 (Ref. 5)	5345 (Ref. 5)	5345 (Ref. 5)	5292 (Ref. 5)	5292 (Ref. 5)	5240 (Ref. 5)	5240 (Ref. 5)
$\varsigma(dd)$	1557 (Ref. 5)	1557 (Ref. 5)	1557 (Ref. 5)	1627 (Ref. 5)	1627 (Ref. 5)	1627 (Ref. 5)	1697 (Ref. 5)	1697 (Ref. 5)	1768 (Ref. 5)	1768 (Ref. 5)	1839 (Ref. 5)	1839 (Ref. 5)
$B_0^2(dd)$	4494 (Ref. 3)		4416 (Ref. 3)	4442 (Ref. 3)		4365 (Ref. 3)		4332 (Ref. 3)		4290 (Ref. 3)		4206 (Ref. 3)
$B_0^4(dd)$	2844 (Ref. 3)	−41595 (Ref. 3)	−17623 (Ref. 3)	2811 (Ref. 3)	−41111 (Ref. 3)	−17418 (Ref. 3)	−40803 (Ref. 3)	−17288 (Ref. 3)	−40407 (Ref. 3)	−17120 (Ref. 3)	−40055 (Ref. 3)	−16784 (Ref. 3)
$B_4^4(dd)$	−21217 (Ref. 3)	−24858 (Ref. 3)	−22558 (Ref. 3)	−20970 (Ref. 3)	−24569 (Ref. 3)	−22296 (Ref. 3)	−24385 (Ref. 3)	−22128 (Ref. 3)	−24148 (Ref. 3)	−21914 (Ref. 3)	−23938 (Ref. 3)	−21484 (Ref. 3)

[a] M^2 and M^4 parameters were included with the ratios $M^2/M^0 = 0.56$ and $M^4/M^0 = 0.31$.
[b] P^4 and P^6 parameters were included with the ratios $P^4/P^2 = 0.5$ and $P^6/P^2 = 0.1$.

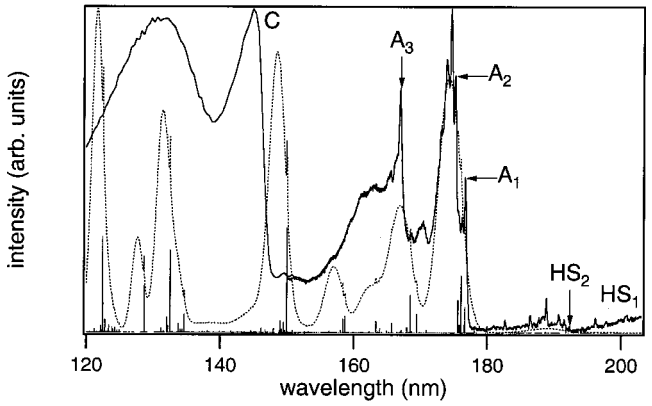

FIG. 5. Excitation spectrum for YPO_4 doped with 1% Dy^{3+} recorded monitoring the $^4F_{9/2} \rightarrow {}^6H_{15/2}$ emission at 478 nm at 10 K.

The first spin-allowed *fd* band shows fine structure and consists of several zero-phonon lines (A_1 to A_3 are indicated) and vibronics. The energy separation between A_1 and A_2 is 475 cm^{-1} and between A_1 and A_3 it is 3290 cm^{-1}. Due to the interaction between the $4f^8$ core and the $5d$ electron, many $4f^8 5d$ levels can be expected in addition to vibronic lines. The distinction between vibronic lines and no-phonon lines is difficult.

On the low-energy side of the spectrum excitation bands corresponding to two spin-forbidden transitions are observed, one around 200 nm (not measured completely, denoted HS_1 in Fig. 5) and one around 190 nm (denoted HS_2 in Fig. 5). The onset of HS_2 is at 192.31 nm (HS_2). The energy difference A_1-HS_2 is 4600 cm^{-1}.

CaF_2. Figure 6 shows the excitation spectrum of CaF_2 doped with 0.005% Dy^{3+} monitoring the $^4F_{9/2} \rightarrow {}^6H_{13/2}$ emission at 590 nm. The onset of the low-spin $4f^8 5d$ excitation band is observed at 172.29 nm (A_1). Spin-allowed transitions to the higher $5d$ crystal-field components are observed around 125 nm (B).

The lowest-energy spin-allowed *fd* band shows fine structure and consists of several zero-phonon lines with (superimposed) vibronic bands. The structure is similar to the pattern observed for Dy^{3+} in YPO_4. Four zero-phonon lines are indicated A_1–A_4. The energy separation between the lines A_1 and A_2 is 725 cm^{-1}, between A_1 and A_3 2090 cm^{-1}, and between A_1 and A_4 3390 cm^{-1}. The splittings are slightly larger than for Dy^{3+} in YPO_4.

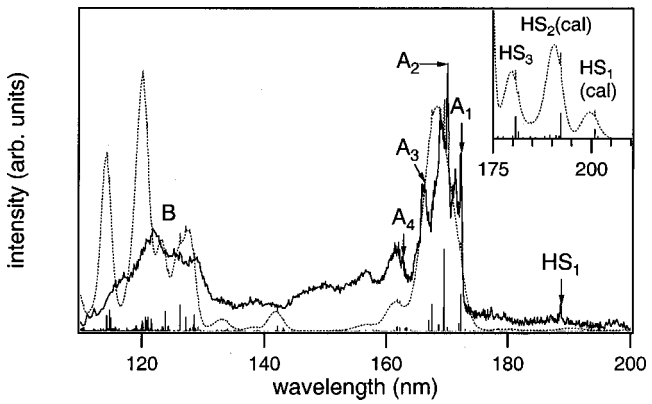

FIG. 6. Excitation spectrum for CaF_2 doped with 0.005% Dy^{3+} recorded monitoring the $^4F_{9/2} \rightarrow {}^6H_{13/2}$ emission at 590 nm at 10 K.

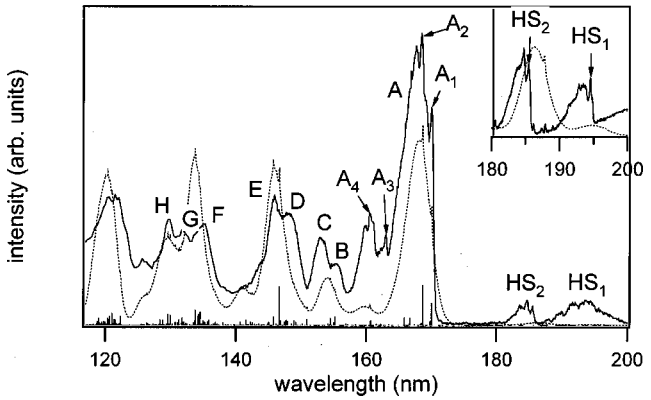

FIG. 7. Excitation spectrum for $LiYF_4$ doped with 1% Dy^{3+} recorded monitoring the $^4F_{9/2} \rightarrow {}^6H_{13/2}$ emission at 575 nm at 10 K. In the inset the excitation spectrum of a 1% single crystal is shown, recorded monitoring all visible $4f^9 \rightarrow 4f^9$ emission at 10 K.

The low intensity band at 188.73 nm (denoted HS_1) may be due to a spin-forbidden *fd* transition. The energy difference between the lowest energy LS and this HS *fd* band is 5050 cm^{-1}. In analogy with $LiYF_4$:Dy^{3+} (see below), a second high-spin *fd* band can be expected around 195 nm. This band is not observed in the present excitation spectrum. In view of the low Dy^{3+} concentration (necessary to avoid cluster sites) the transition to the lower-energy high-spin state may be too weak to be observed. Some of the weak sharp lines between 170 and 205 nm may not be due to $4f^9 \rightarrow 4f^8 5d$ (HS) lines, but to high-energy transitions within the $4f^9$ configuration. For example, the line at 188.73 nm may also be due to a transition to the $^2K(2)_{17/2}$ level.[18]

$LiYF_4$. Figure 7 shows the excitation spectrum of the Dy^{3+} $^4F_{9/2} \rightarrow {}^6H_{13/2}$ emission (at 575 nm) in powdered $LiYF_4$ doped with 1% Dy^{3+}. The LS *fd* onset is observed at 170.13 nm (A_1). Spin-allowed transitions to the higher $5d$ crystal-field components are observed at 148 nm (D), 135 nm (F), 132 nm (G), and 130 nm (H).

The lowest-energy spin-allowed *fd* band (A) shows fine structure and consists of zero-phonon lines and (superimposed) vibronic bands. The structure is similar to the structure observed in the lowest-energy *fd* band of Dy^{3+} in CaF_2 and YPO_4. Four zero-phonon lines could be identified, numbered A_1–A_4. The energy separation between the lines A_1 and A_2 is 560 cm^{-1}, between A_1 and A_3 2560 cm^{-1}, and between A_1 and A_4 3480 cm^{-1}, which is similar to the splittings observed in YPO_4 and CaF_2.

Around 193 and 185 nm two spin-forbidden *fd* transitions are observed. In the inset of Fig. 7 the excitation spectrum of a 1% single crystal sample is shown in this wavelength region. The zero-phonon lines HS_1 and HS_2 are observed at 194.56 and 185.44 nm, respectively. The energy difference between the two high-spin bands is about 2500 cm^{-1}, similar to the A_1-A_3 splitting of the first low-spin *fd* band. The energy separation between the lowest-energy LS and HS *fd* band is about 7380 cm^{-1}.

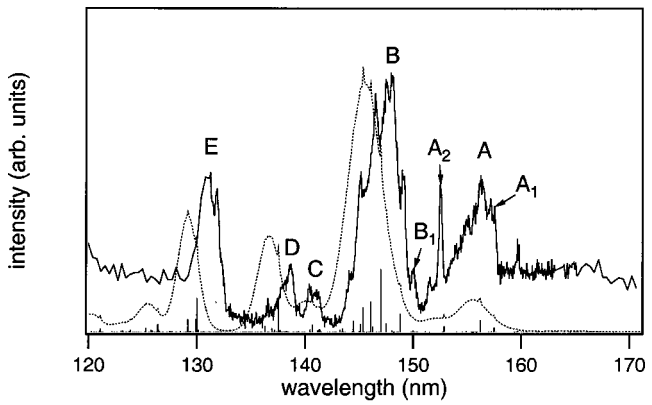

FIG. 8. Excitation spectrum for CaF_2 doped with 0.001% Ho^{3+} recorded monitoring all visible emissions (500–800 nm) at 10 K.

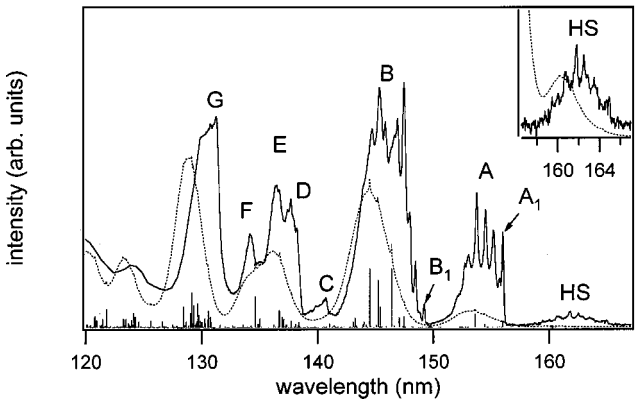

FIG. 9. Excitation spectrum for $LiYF_4$ doped with 1% Ho^{3+} recorded monitoring the $^5S_2 \rightarrow {}^5I_8$ emission at 541 nm at 10 K.

2. Model

The simulated spectra are shown as the dotted lines in Figs. 5, 6, and 7 and the positions of electronic origins are indicated by vertical lines. The agreement between experiment and model is good. The calculated splitting between the low-spin and high-spin *fd* states is slightly larger than the experimentally observed splitting. The fact that two high-spin *fd* states are observed on the low-energy side of the low-spin *fd* bands is reproduced by the calculations. The relative intensity of the transitions to the lowest-energy high-spin state is lower, which can explain the fact that we could not observe the lowest-energy HS state in the excitation spectrum of Dy^{3+} in CaF_2 due to the very low Dy^{3+} concentration in this crystal. All experimentally observed bands can be assigned. The relative intensity of the spin-forbidden transitions is higher than calculated. A possible explanation is that the spin-selection rule is partly lifted by mechanisms (for example, mixing of low-spin and high-spin *fd* states) not included in the present model. It is also possible that the absorption of the LS transition is saturated. It is known that saturation effects in the excitation spectra of rare-earth ions can be significant at low concentrations (0.5%), even in powder samples.[19]

C. Ho^{3+}

YPO_4. In YPO_4, no Ho^{3+} emission can be observed. Energy gaps between the $4f^{10}$ states do not exceed 5000 cm^{-1} (Refs. 18, 20). Due to the high phonon energy of phosphate vibrations ($\sim$1200 cm^{-1}) all gaps can be bridged by less than five phonons. In this case nonradiative multiphonon relaxation dominates over radiative decay. Naturally, excitation spectra cannot be recorded if there is no emission.

CaF_2. Figure 8 shows the excitation spectrum for CaF_2 doped with 0.001% Ho^{3+} recorded monitoring all visible emissions (500–800 nm). A number of structured bands are observed with maxima at 156 nm (A), 147 nm (B), 141 nm (C), 139 nm (D), and 131 nm (E). These bands are all assigned to transitions to excited *fd* levels involving the lowest-energy $5d$ crystal-field component. Transitions to the $^2T_2$ levels are expected around 122 nm, but at these wavelengths ($<$125 nm) host lattice absorption is large and as a consequence the high energy *fd* bands cannot be observed.

Band A shows fine structure and consists of zero-phonon lines (indicated A_1-A_2) and vibronic lines. The *fd* onset is at 157.5 nm (A_1), the energy difference between A_1 and A_2 is 2090 cm^{-1}. Band B also shows a pronounced structure. This band has an onset at 150 nm (B_1), the energy difference between A_1 and B_1 is 3180 cm^{-1}.

No spin-forbidden transitions are observed on the low-energy side of the lowest-energy spin-allowed *fd* band in this spectrum, due to the low Ho^{3+} concentration. The weak line observed at 159 nm may be due to a transition to a high-energy $4f$ level of Ho^{3+}.

$LiYF_4$. Figure 9 shows the excitation spectrum of the Ho^{3+} emission at 541 nm in powdered $LiYF_4$ doped with 1% Ho^{3+}. A number of broad bands are observed, some of which show fine structure (A, B, C, D). The low-spin *fd* onset is at 156.0 nm (A_1). On the low-energy side of the spectrum, a pronounced structure is observed in bands with maxima at 155 nm (A) and 146 nm (B). These bands consist of zero-phonon lines (e.g., A_1 and B_1) and vibronic lines. Band A and B are both assigned to spin-allowed transitions to states involving the lowest-energy $5d$ crystal-field component. The energy difference between the zero-phonon lines A_1 and B_1 is 2920 cm^{-1}, which is similar to the separation A_1-B_1 in CaF_2.

Comparison of the excitation spectra of Ho^{3+} in $LiYF_4$ and CaF_2 shows more similarities. The splitting of the four lowest-energy bands A–D is very similar: the energy differences of the onset of the bands B–D and A are 3180 cm^{-1} (CaF_2) and 2920 cm^{-1} ($LiYF_4$) for B, 7250 cm^{-1} (CaF_2) and 6975 cm^{-1} ($LiYF_4$) for C, and 8610 cm^{-1} (CaF_2) and 8260 cm^{-1} ($LiYF_4$) for D. Also the fine structure within the bands is similar for Ho^{3+} in CaF_2 and $LiYF_4$. This observation is not surprising, since the fine structure within the bands is due to splitting of the $4f^{n-1}$ core and *f-d* interaction. This will be very similar for Ho^{3+} in the two fluoride host lattices.

The low intensity band with a maximum at 162 nm (HS) is assigned to the lowest-energy spin-forbidden *fd* transition. The band shows fine structure and consists of a zero-phonon line at 164.9 nm and a vibronic side band. The energy separation between the first LS and first HS *fd* bands is 3470 cm^{-1}.

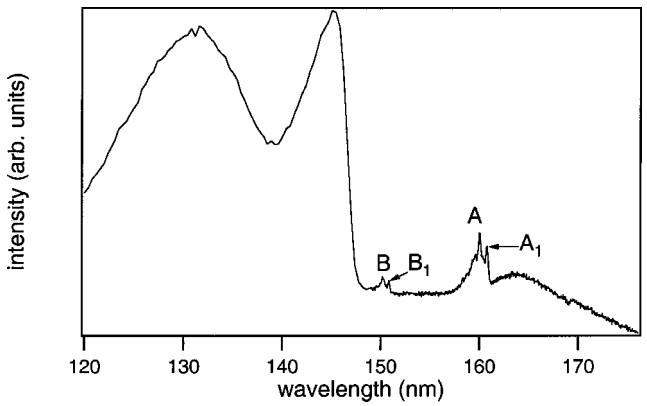

FIG. 10. Excitation spectrum for YPO_4 doped with 1% Er^{3+} recorded monitoring the $^2H_{9/2} \rightarrow {}^4I_{15/2}$ emission at 400 nm at 10 K.

D. Er^{3+}

YPO_4. The excitation spectrum of the Er^{3+} ($4f^{11}$) $^2H_{9/2} \rightarrow {}^4I_{15/2}$ emission at 400 nm in YPO_4 doped with 1% Er^{3+} is shown in Fig. 10. In this spectrum only two *fd* bands are observed with maxima at 160 nm (A) and 150 nm (B). Host lattice excitation bands are observed at wavelengths shorter than 144 nm. The band at 162 nm is probably due to a defect in the lattice, which upon excitation transfers energy to Er^{3+} or emits around 440 nm.

The lowest-energy LS *fd* band (A) shows fine structure. It consists of zero-phonon lines and vibronic lines. The *fd* onset (A_1) is at 160.8 nm. Band B also shows fine structure, zero-phonon line B_1 is observed at 150.84 nm. The energy separation A_1-B_1 is 4110 cm^{-1}.

CaF_2. Figure 11 shows the excitation spectrum of the Er^{3+} *fd* emission at 167 nm for a CaF_2 single-crystal doped with 0.001% Er^{3+}. Structured bands are observed with maxima at 155 nm (A), 146 nm (B), 135 nm (C), and 130 nm (D). Transitions to the $4f^{10}5d(^2T_2)$ levels are expected around 120 nm and are not observed in the excitation spectrum due to competing host lattice absorption at wavelengths shorter than 125 nm.

The lowest-energy LS *fd* band (A) shows fine structure, the zero-phonon line A_1 is located at 156.05 nm. Other zero-phonon lines are observed at 146.33 nm (B_1), 135.42 nm (C_1), and 130.13 nm (D_1). Energy separations A_1-B_1, A_1-C_1, and A_1-D_1 are 4260, 9760, and 12 760 cm^{-1}, respectively. The energy separation between the zero-phonon lines A_1 and B_1 is similar to the energy difference between these lines for Er^{3+} in YPO_4 (4110 cm^{-1}).

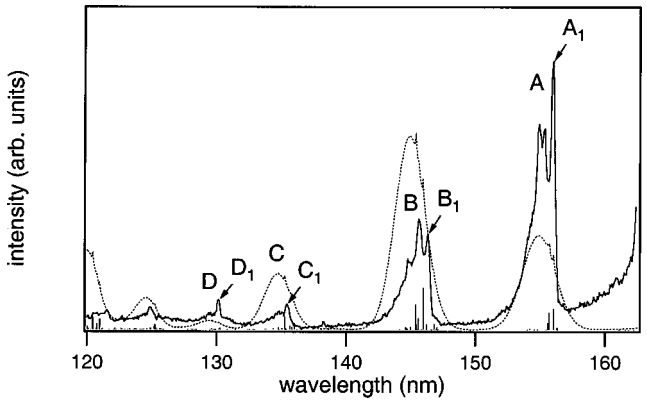

FIG. 11. Excitation spectrum for CaF_2 doped with 0.001% Er^{3+} recorded monitoring the *fd* emission at 167 nm at 10 K.

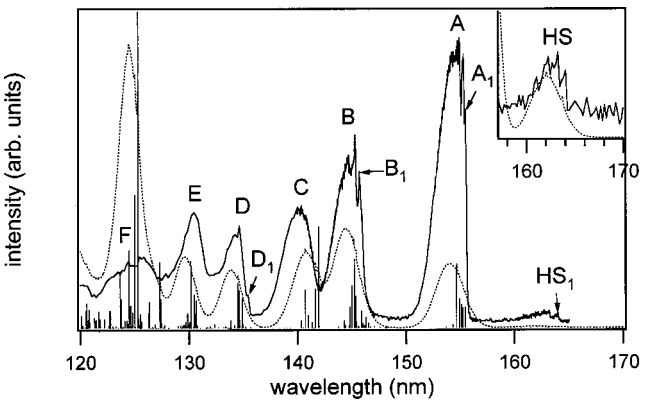

FIG. 12. Excitation spectrum for $LiYF_4$ doped with 1% Er^{3+} recorded monitoring the $^4S_{3/2} \rightarrow {}^4I_{15/2}$ emission at 550 nm at 10 K.

Spin-forbidden *fd* bands are not observed in the excitation spectrum of CaF_2:Er^{3+}, due to the low dopant concentration (0.001%). The increasing intensity at wavelengths longer than 160 nm is caused by scattered excitation radiation (the spectrum is recorded for Er^{3+} emission at 167 nm).

$LiYF_4$. Figure 12 shows the excitation spectrum of the Er^{3+} $^4S_{3/2} \rightarrow {}^4I_{15/2}$ emission at 550 nm for powdered $LiYF_4$ doped with 2% Er^{3+}. A number of broad bands are observed, some of which show fine structure. The first spin-allowed *fd* transition is observed at 155 nm (A). Transitions to higher $5d$ crystal-field components are observed at 140 nm (C) and 126 nm (F). Bands A and B both show fine structure. The bands consist of zero-phonon lines (A_1 and B_1) at 155.5 nm, respectively, 145.7 nm. A third structured band can be observed with a zero-phonon line at 135.4 nm (D_1). The energy separation between the zero-phonon lines A_1 and B_1 is 4330 cm^{-1}, between D_1 and A_1 9465 cm^{-1}. This is similar to the separation between the no-phonon lines of bands *A*, *B*, and *C* in the spectrum of CaF_2:Er^{3+} and suggests that the origin of these bands in CaF_2 and $LiYF_4$ is the same. In CaF_2 these bands were assigned to transitions to the ^2E levels while the transitions to the $^2T_2$ levels were expected at much higher energy (at about 120 nm). Therefore, also in $LiYF_4$ these bands can be assigned to transitions to the $4f^{10}5d$ states involving the lowest-energy $5d$ crystal-field component.

The low intensity band with a maximum at 163 nm and a zero-phonon line at 164 nm (HS_1) is assigned to the lowest-energy spin-forbidden *fd* transition of Er^{3+}. The energy difference between the transition to the LS and HS *fd* state is 3335 cm^{-1}, again smaller than the HS-LS splitting observed for Tb^{3+}, Dy^{3+}, and Ho^{3+}.

E. Tm^{3+}

YPO_4. Figure 13 shows the excitation spectrum of the Tm^{3+} $^1D_2 \rightarrow {}^3H_6$ emission (342 nm) for YPO_4 doped with

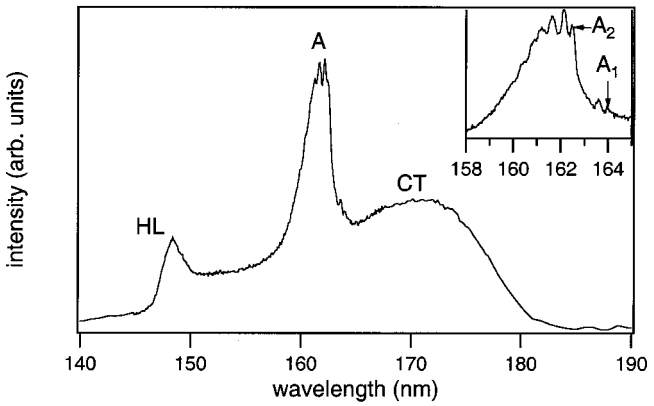

FIG. 13. Excitation spectrum for YPO_4 doped with 1% Tm^{3+} recorded monitoring the $^1D_2 \rightarrow {}^3H_6$ emission at 342 nm at 10 K.

1% Tm^{3+}. The first LS *fd* band has a maximum at 162 nm (A). Similar to Sm^{3+} $(4f^5)$ and Eu^{3+} $(4f^6)$ (Ref. 3), the charge transfer (CT) state of Tm^{3+} $(4f^{12})$ is located at lower energy than the lowest-energy *fd* state in an oxide, and has a maximum at 171 nm. Unfortunately, the broad charge transfer band overlaps the first LS *fd* band and prohibits the observation of the weak HS *fd* band. Below 144 nm, the YPO_4 host lattice (HL) absorbs. In the excitation spectrum the onset of the host lattice absorption is observed as a steep decrease. Since host lattice absorption is a competing absorption which does not result in the emission that is monitored (due to inefficient energy transfer from the host lattice to the emitting *fd* state of Tm^{3+}) the signal decreases for wavelengths shorter than 144 nm. In the inset in Fig. 13 band A is shown in more detail. The band shows fine structure, zero-phonon line A_1 is observed at 164.0 nm.

CaF_2. Figure 14 shows the excitation spectrum of the Tm^{3+} fd emission (at 166 nm) for CaF_2 doped with 0.001% Tm^{3+}. Structured excitation bands are observed with maxima at 156 nm (A), 142 nm (B), and 133 nm (C). These bands are assigned to transitions to $4f^{11}5d$ states involving the ^2E levels. Transitions to the higher $5d$ crystal-field states $(^2T_2)$ are expected at wavelengths shorter than 121 nm and are not observed in the spectrum due to competing host lattice absorption at wavelengths shorter than 125 nm.

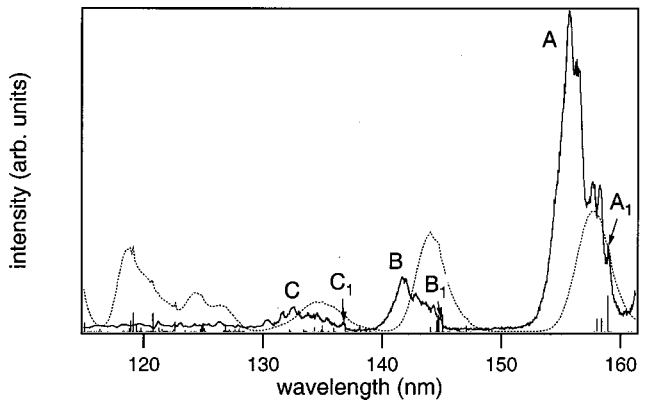

FIG. 14. Excitation spectrum for CaF_2 doped with 0.001% Tm^{3+} recorded monitoring the *fd* emission at 166 nm at 10 K.

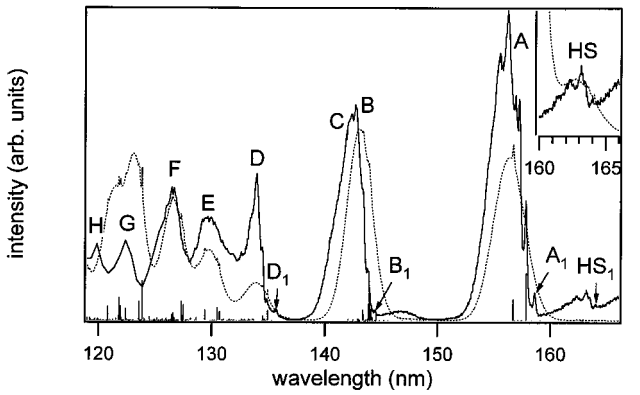

FIG. 15. Excitation spectrum for $LiYF_4$ doped with 1% Tm^{3+} recorded monitoring the *fd* emission at 170 nm at 10 K.

The first spin-allowed *fd* band shows fine structure. It consists of some lines of low intensity, followed by more intense lines, similar to the observation for Tm^{3+} in YPO_4. The first zero-phonon line is observed at 158.96 nm (A_1). Band B and band C also show fine structure. They start with the zero-phonon lines B_1 (at 144.92 nm) and C_1 (at 136.82 nm), respectively. The energy separation $A_1 - B_1$ is 6090 cm^{-1}, $A_1 - C_1$ is 10 240 cm^{-1}. Transitions to HS *fd* states are not observed in the spectrum due to the low Tm^{3+} concentration.

$LiYF_4$. Figure 15 shows the excitation spectrum of the Tm^{3+} fd emission (at 170 nm) for powdered $LiYF_4$ doped with 1% Tm^{3+}. The spectrum consists of a number of broad bands. The lowest-energy LS *fd* band has a maximum at 156 nm (A), transitions to higher $5d$ crystal-field components are observed at 142 nm (C), 127 nm (F), 122 nm (G), and 120 nm (H).

The spin-allowed transition to the lowest-energy *fd* state shows fine structure. The *fd* onset (indicated by zero-phonon line A_1) is observed at 158.61 nm. The fine structure pattern is similar to the patterns of the lowest-energy Tm^{3+} fd band observed in YPO_4 and CaF_2; some lines of low intensity, followed by more intense lines. This similarity between the patterns in the different host lattices confirms that the structure is due to the $4f^{n-1}$ core and f-d interaction which is similar for Tm^{3+} in the different host lattices. The influence of the host lattice (crystal-field splitting and vibrational frequencies) on the structure in the lowest-energy spin-allowed *fd* excitation band is less important.

On the low-energy side of band C, denoted in the spectrum by the zero-phonon line B_1, fine structure is observed. Also band D, at 134 nm, shows fine structure. The positions of the structured bands (relative to A) are similar to the positions of bands B and C relative to A for Tm^{3+} in CaF_2 (where only transitions to the lowest-energy $5d$ crystal-field state were observed) and are therefore assigned to transitions to $4f^{11}5d$ levels involving the lowest-energy $5d$ crystal-field component of Tm^{3+} in $LiYF_4$. The energy separation between the zero-phonon lines A_1 and B_1 is 6185 cm^{-1}, between A_1 and D_1 10 690 cm^{-1}, very similar to the values reported above for Tm^{3+} in CaF_2.

The lowest-energy spin-forbidden *fd* transition is observed at 163 nm and does also show fine structure. The

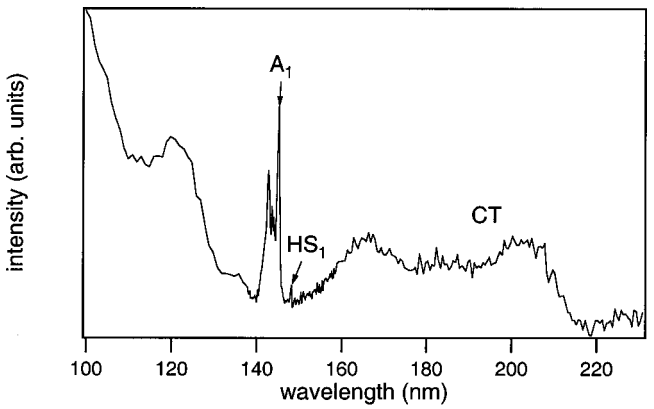

FIG. 16. Excitation spectrum for $LuPO_4$ doped with 1% Yb^{3+} recorded monitoring the charge transfer emission at 300 nm at 10 K.

zero-phonon line is observed at 164 nm (HS_1), the energy difference between the LS and HS *fd* state is 2050 cm^{-1}. This is the smallest energy separation between the LS and HS *fd* state of all heavy lanthanides discussed up to now.

F. Yb^{3+}

$LuPO_4$. The $4f^n \rightarrow 4f^{n-1}5d$ transitions of Yb^{3+} are observed at high energy. To measure the *fd* excitation spectrum, the Yb^{3+} ion was incorporated in $LuPO_4$ instead of YPO_4, because the host lattice absorption starts at higher energy for $LuPO_4$ (host lattice excitation edge $LuPO_4 \sim 140$ nm, $YPO_4 \sim 144$ nm). Just as for Eu^{3+}, Sm^{3+}, and Tm^{3+} the charge transfer (CT) absorption is at lower-energy than the lowest-energy *fd* absorption band. Figure 16 shows the excitation spectrum of $LuPO_4$:Yb^{3+} monitoring the charge transfer emission at 300 nm (Ref. 12).

On the low-energy side of the spectrum, the charge transfer absorption band is observed with the lowest-energy maximum at about 205 nm. The onset of the spin-allowed *fd* bands is observed as a zero-phonon line at 145.24 nm (denoted A_1 in the spectrum). At 148.3 nm, another zero-phonon line is observed (HS_1), which may be due to a spin-forbidden $4f^n \rightarrow 4f^{n-1}5d$ transition on Yb^{3+}. The splitting HS-LS would then be 1400 cm^{-1}, which is in line with the decrease in HS-LS splitting observed from Tb^{3+} ($\sim$8000 cm^{-1}) to Tm^{3+} ($\sim$2000 cm^{-1}).

CaF_2 and $LiYF_4$. In CaF_2 and $LiYF_4$ no efficient UV or visible Yb^{3+} emission is observed which can be monitored to record an excitation spectrum. Absorption spectra for Yb^{3+} in CaF_2 have been reported in the literature,[15] the lowest-energy $4f^n \rightarrow 4f^{n-1}5d$ zero-phonon line was observed at 142 nm. At about 145 nm, structure was observed on top of the broad charge transfer band. This structure may be due to a spin-forbidden *fd* transition on Yb^{3+}. The energy splitting between the lowest-energy low-spin and high-spin *fd* band would be about 1500 cm^{-1}, which is in line with the observation for $LuPO_4$:Yb^{3+}. The intensity of the transition, which is observed on top of the charge transfer band is rather high for a spin-forbidden transition. A possible explanation for the higher intensity is stronger mixing of the high spin *fd* state and the lowest-energy LS *fd* state, due to the smaller energy difference between the LS and HS states for Yb^{3+}.

IV. GENERAL DISCUSSION

High-resolution $4f^n \rightarrow 4f^{n-1}5d$ excitation spectra have been recorded for the heavy lanthanide ions ($n>7$) incorporated in YPO_4, CaF_2, and $LiYF_4$. Similar to the observation for the light ($n<7$) lanthanides,[3] the transition to the lowest-energy $5d$ crystal-field component shows fine structure. For transitions to energy levels corresponding to higher energy $5d$ crystal-field components the fine structure has disappeared and broad structureless bands are observed. The absence of fine structure is explained by a fast photoionization process if the higher energy $5d$ levels are located in the conduction band. Heisenberg broadening of the electronic transitions broadens the sharp zero-phonon and vibronic lines and fine structure is lost.

Comparison of the fine structure observed for transitions involving the lowest-energy $5d$ level shows that the structure is very similar for one type of rare-earth ion in the three different host lattices. The fine structure is due to interactions in the $4f^{n-1}$ core and the Coulomb and exchange interactions between the $4f$ electrons and the $5d$ electron and these are not strongly dependent on the host lattice. Differences occur at higher energies due to differences in the $5d$ crystal-field splitting in the three host lattices.

The crystal-field splitting becomes smaller for the heavier lanthanide ions as a result of the lanthanide contraction. In the $4f^1 \rightarrow 5d^1$ and $4f^8 \rightarrow 4f^7 5d^1$ excitation spectra the different crystal-field components can be most clearly observed due to the absence of splitting of the $4f^{n-1}$ core (Ce^{3+},$4f^0$ core) or a very large energy difference to the first excited state of the core (Tb^{3+},$4f^7$ core). Comparison of the excitation spectra of Ce^{3+} and Tb^{3+} in the different host lattices indicates that the crystal-field splitting for the $5d$ state of Tb^{3+} is about 3–5 % smaller than for Ce^{3+}. Further analysis of the excitation spectra of the other heavy lanthanides indicates a continuous decrease of the crystal-field splitting to 91% of the Ce^{3+} splitting for Tm^{3+}.

For the heavy lanthanide ions, spin-forbidden *fd* excitation bands are observed in addition to spin-allowed *fd* bands. Similar to the spin-allowed *fd* bands, the transition to the lowest-energy high-spin $5d$ crystal-field component shows fine structure. The energy separation between the first spin-allowed *fd* band and the first spin-forbidden *fd* band decreases through the series. The observed splitting is largest for Tb^{3+} (about 7700 cm^{-1}) and decreases to about 2000 cm^{-1} for Tm^{3+}. This indicates that the exchange interaction between the $4f^{n-1}$ core and the $5d$ electron decreases with increasing nuclear charge of the rare-earth ion. Possible explanations for the decrease in splitting between the lowest energy HS and LS states with increasing nuclear charge of the heavy rare earth ions are discussed in Ref. 21.

To compare the experimentally observed spectra with energy-level calculations a relatively simple model is used with as input parameters the $5d$ crystal-field parameters (estimated from the splitting of the $5d$ electron), parameters for the splitting of the $4f^{n-1}$ core and parameters for the spin-

orbit coupling of the $5d$ electron and the Coulomb interaction between the $4f$ and $5d$ electrons. The *f-d* interaction parameters are calculated using Cowan's program[5] (for the free ion), but are reduced in order to correct for the delocalization of the $5d$ electron over the ligands in a solid. From the spectra of the heavy lanthanides a good estimate for the reduction of the *f-d* interaction can be obtained. Due to the exchange interaction between the $4f^{n-1}$ core and the $5d$ electron a high-spin and low-spin $4f^{n-1}5d$ state arise. The splitting between the high-spin and low-spin *fd* states depends on the *f-d* interaction parameters. From the observed HS-LS splitting in the excitation spectrum of Tb^{3+} in $LiYF_4$, the *f-d* interaction parameters were estimated to be about 67% of the calculated values. In the spectra of the heavy lanthanides in CaF_2, no spin-forbidden transitions to the high-spin *fd* states were observed (except for CaF_2:Tb^{3+}) due to the low concentration of lanthanides in these crystals (to prevent the formation of cluster sites which occur at higher concentrations). In view of the similar covalency of $LiYF_4$ and CaF_2 (both fluoride host lattices) a reduction to 67% of the calculated parameters was used for CaF_2. The YPO_4 host lattice is more covalent, which increases the delocalization of the $5d$ electron over the ligands. From the smaller splitting between the high-spin and low-spin states of Tb^{3+} in YPO_4 as compared to $LiYF_4$ (7370 cm^{-1} in YPO_4, 7995 cm^{-1} in $LiYF_4$), a reduction of the *f-d* interaction parameters to 60% of the calculated values was estimated for the lanthanides in YPO_4.

The agreement between the experimentally observed spectra and the energy-level calculations is good. The observed structure and relative intensities of the *fd* transitions are reproduced by the calculations. Especially for the lower-energy bands, the agreement between experiment and theory is good and fine structure in the spectra is reproduced by the calculations. At higher energies there are discrepancies, especially for lanthanides in $LiYF_4$. This was also observed for the light lanthanides[3] and is partly due to the fact that the $5d$ crystal-field splitting for the three highest crystal-field components cannot be reproduced by the fit for Ce^{3+} in $LiYF_4$. Also host lattice absorption interferes at high energies. The presence of both high-spin and low-spin *fd* states is predicted by the theory. The splitting between the high-spin and low-spin states decreases through the series from almost 8000 cm^{-1} for Tb^{3+} to just over 2000 cm^{-1} for Tm^{3+}. There is a good agreement between the calculated HS-LS splittings and the experimentally observed splittings. The calculated intensity of the HS bands is often lower than experimentally observed. This may be due to relaxation of the spin-selection rule by a mechanism not included in our model. An alternative explanation for this is saturation of the absorption. It is known that saturation effects can be significant at low RE dopant concentrations (0.5%) even in powder samples.[19]

Although since our previous papers[2,3] many of the suggested improvements to the theory have been made in this paper (such as decreasing the $5d$ crystal-field parameters and *fd* Coulomb parameters), still further improvements are possible. For example, the different *f-d* interaction parameters $F^2(fd)$, $F^4(fd)$, $G^1(fd)$, $G^3(fd)$, and $G^5(fd)$ have a different influence on the position of the calculated *fd* levels, and in order to reproduce all experimentally observed zero-phonon lines, a fine-tuning of the individual parameters is necessary. Up until now, we have kept the ratio of the *f-d* parameters constant and reduced all *f-d* interaction parameters to 67% of the calculated value (for $LiYF_4$ and CaF_2). This is not necessarily correct. For example, the *f-d* interaction parameters that Sugar obtained after a least square fit to the $4f5d$ spectrum of the Pr^{3+} ion in the vapor state show especially for $F^2(fd)$ a much smaller value[22] (about 66% of the calculated value). We have also studied the influence of the five *f-d* interaction parameters on the HS-LS splitting. To do this, splitting of the lowest-energy *fd* levels was calculated as one of the $4f5d$ atomic parameters [either $F^2(fd)$, $F^4(fd)$, $G^1(fd)$, $G^3(fd)$, or $G^5(fd)$] were increased from zero to the values predicted for the free ion (according to Cowan's program[5]), while all other parameters are kept at a constant (free ion) value. These calculations show that most of the variation in the splitting between the high-spin and low-spin states is caused by the $G^k(fd)$ parameters, especially by $G^1(fd)$ and $G^5(fd)$. Until enough spectral information is obtained to unambiguously identify the identity of the spectral lines it is not possible to determine the values of the individual parameters. Polarization dependent measurements will provide information on the symmetry of the levels and can provide support for the assignment of experimentally observed levels to calculated levels. For Pr^{3+} in $LiYF_4$ a thorough study has been performed,[1] but more work on other ions is necessary to be certain of the correctness of the parameters. In addition, we have used for the $4f^{n-1}5d$ configuration literature values for the parameters in $H_A(ff)$ for the same ion multiplied by a small factor ($\sim$1.06, based on the ratio between the calculated values for the $4f^{n-1}5d$ and $4f^n$ configurations). This might not be correct, but at the moment there is not enough information in the spectra to definitively test the effect of varying these parameters.

We have developed a relatively simple model to explain the *fd* excitation spectra of the lanthanide ions. This model requires only a small number of adjustable parameters and has now been applied to successfully simulate the *fd* excitation spectra through the entire lanthanide series.

V. CONCLUSION

In this paper, an overview of the $4f5d$ excitation spectra of the heavy lanthanides (Tb^{3+}, Dy^{3+}, Ho^{3+}, Er^{3+}, Tm^{3+}, and Yb^{3+}) in YPO_4, CaF_2, and $LiYF_4$ has been given. Spin-forbidden transitions as well as spin-allowed transitions are observed for all heavy lanthanides. The splitting between the low-spin and high-spin *fd* state decreases with increasing nuclear charge of the lanthanide ion. Fine structure is observed for the transitions to levels involving the lowest-energy $5d$ crystal-field component.

The structure in the *fd* excitation spectra of the lanthanides is calculated using a theoretical model that extends established models for the $4f^n$ configuration by including crystal-field and spin-orbit interactions for the $5d$ electron and the Coulomb interaction between the $4f$ and $5d$ electrons. Calculations of the positions of the $4f^{n-1}5d$ energy levels are compared with the experimental data. A good

agreement is obtained between experimental and simulated spectra using parameters for the splitting of the $5d$ state (from the Ce^{3+} spectra), the $4f^{n-1}$ splitting (from the literature) and the *f-d* Coulomb interaction (calculated for the free ion using Cowan's code). The $5d$ crystal-field parameters were slightly reduced to account for the slight reduction of the crystal-field splitting for the heavier rare earth ions ($\sim$9% between Ce^{3+} and Tm^{3+}). The *f-d* interaction parameters are reduced to 67% of the calculated free ion value for the fluorides and to 60% of the calculated value for the phosphates to correct for the nephelauxetic effect. The larger reduction of the *f-d* interaction parameters in the phosphates is in line with the larger covalency of the phosphate host lattice as compared to the fluoride lattice. The presence of both high-spin and low-spin *fd* states and the trend that the splitting between the high-spin and low-spin states decreases through the series is reproduced by the theory.

ACKNOWLEDGMENTS

The authors wish to thank Dr. G. D. Jones of the University of Canterbury (Christchurch, New Zealand) for doing FTIR measurements on the CaF_2 crystals and many helpful discussions concerning the spectroscopy on doped CaF_2 crystals. The authors are grateful to Dr. P. Gürtler and Dr. S. Petersen from HASYLAB for the opportunity to use the excellent facilities for VUV spectroscopy at the DESY synchrotron, Hamburg (Germany) and their support whenever needed. The financial support of Philips Lighting and the New Zealand Marsden Fund (Contract No. UOC704) is gratefully acknowledged.

[1] M. Laroche, J.-L. Doualan, S. Girard, J. Margerie, and R. Moncorgé, J. Opt. Soc. Am. B **17**, 1291 (2000).
[2] M. F. Reid, L. van Pieterson, R. T. Wegh, and A. Meijerink, Phys. Rev. B **62**, 14744 (2000).
[3] L. van Pieterson, M. F. Reid, S. Soverna, R. T. Wegh, and A. Meijerink, Phys. Rev. B **65**, 045113 (2002) (the preceding paper).
[4] J. L. Ryan and C. K. Jørgensen, J. Phys. Chem. **70**, 2845 (1966).
[5] R. D. Cowan, in *The Theory of Atomic Structure and Spectra* (University of California Press, Berkeley, 1981)
[6] C. Görller-Walrand and K. Binnemans, in *Handbook on the Physics and Chemistry of Rare Earths*, edited by J. K. A. Gschneider and L. Eyring (North-Holland, Amsterdam, 1996), Vol. 23, pp. 121–283.
[7] K. Lesniak, J. Phys.: Condens. Matter **2**, 5563 (1990).
[8] G. M. Williams, P. C. Becker, J. G. Conway, N. Edelstein, L. A. Boatner, and M. M. Abraham, Phys. Rev. B **40**, 4132 (1989).
[9] W. T. Carnall, G. L. Goodman, K. Rajnak, and R. S. Rana, J. Chem. Phys. **90**, 3443 (1989).
[10] H. A. Weakliem, Phys. Rev. B **6**, 1743 (1972).
[11] T. Hoshina and S. Kuboniwa, J. Phys. Soc. Jpn. **31**, 828 (1971).
[12] L. van Pieterson, M. Heeroma, E. de Heer, and A. Meijerink, J. Lumin. **91**, 177 (2000).
[13] B. M. Tissue and J. C. Wright, Phys. Rev. B **36**, 9781 (1987).
[14] J. Corish, C. R. A. Catlow, P. W. M. Jacobs, and S. H. Ong, Phys. Rev. B **25**, 6425 (1982).
[15] T. Szczurek and M. Schlesinger, in *Rare Earths Spectroscopy*, edited by B. Jezowska-Trzebiatowska, J. Legendziewicz, and W. Strek (World Scientific, Singapore, 1985).
[16] L. van Pieterson, M. F. Reid, and A. Meijerink (unpublished).
[17] M. Marsman, J. Andriesen, and C. W. van Eijk, Phys. Rev. B **61**, 16477 (2000).
[18] R. T. Wegh, A. Meijerink, R. J. Lamminmäki, and J. Hölsä, J. Lumin. **87–89**, 1002 (2000).
[19] C. de Mello Donéga, A. Meijerink, and G. Blasse, J. Lumin. **62**, 189 (1994).
[20] G. H. Dieke, in *Spectra and Energy Levels of Rare Earth Ions in Crystals* (Interscience, New York, 1968).
[21] L. van Pieterson, M. F. Reid, R. T. Wegh, and A. Meijerink, J. Chem. Phys. **115**, 9382 (2001).
[22] J. Sugar, J. Opt. Soc. Am. **55**, 1058 (1965).